Mineralogical Magazine, June 2005, Vol. 69(3), pp. 345–358

Hydrogen and minor element incorporation in synthetic rutile

G. D. BROMILEY[1,2,*] AND N. HILAIRET[3]

[1] Bayerisches Geoinstitut, Universität Bayreuth, 95440 Bayreuth, Germany
[2] Department of Earth Sciences, University of Cambridge, Downing Street, Cambridge CB2 3EQ, UK
[3] Laboratoire de Sciences de la Terre, ENS-Lyon, 46 Alleé d'Italie, 69364 Lyon, Cedex 07, France

ABSTRACT

The solubility and incorporation mechanisms of H and various trivalent and divalent cations in synthetic rutile have been investigated. Experiments performed using different bulk Fe_2O_3 contents demonstrate that Fe^{3+} substitutes onto the main Ti site, charge-balanced by oxygen vacancies. Under more reducing conditions in Fe-poor systems, the concentration of Ti interstitials in rutile is increased, resulting in a decrease in H solubility. Variation in the solubility of different oxides in rutile as a function of ionic radius implies substitution onto the main Ti site, probably charge-balanced by oxygen vacancies. To a lesser degree, substitution of trivalent and divalent cations is locally charge-balanced by H incorporation. Variation in OH-stretching frequencies in infrared spectra as a function of composition implies that octahedral defects and structurally-incorporated H are coupled. However, in all samples, some of the H is also decoupled from substitutional impurities, as is evident from an OH-absorption band at 3279 cm^{-1}. This band corresponds to the main OH band seen in spectra of many natural rutiles, implying that in most rutiles, H defects are decoupled from substitutional defects.

KEYWORDS: rutile, hydrogen, substitution, solubility, spectroscopy.

Introduction

RUTILE is the most common, naturally occurring form of titanium oxide (TiO_2), and is an accessory mineral in many igneous and metamorphic rocks. In high-pressure and ultra-high-pressure eclogites, modal percentages of rutile may reach several wt.%. Rutile has a simple tetragonal structure, with each Ti^{4+} ion surrounded by six oxygens at the corners of a slightly distorted, regular octahedron, and each oxygen surrounded by three Ti^{4+} ions lying in a plane at the corners of an approximately equilateral triangle (Deer *et al*., 1992). Rutile can contain variable amounts of pentavalent (Nb^{5+}, Ta^{5+}), trivalent (Fe^{3+}, Al^{3+}, Cr^{3+}) and, to a lesser degree divalent (Mg^{2+}, Ca^{2+}) cations. Coupled substitution of pentavalent and trivalent cations onto Ti^{4+} sites maintains charge neutrality. In addition, substitution of lower-valence cations may be charge-balanced by incorporation of hydrogen in the rutile structure (Johnson *et al.*, 1968). Studies of natural rutiles from various geological terrains have also demonstrated the great affinity of rutile for hydrogen incorporation, and rutile is one of the most 'hydrous' nominally-anhydrous minerals (NAMs) so far identified (Rossman and Smyth, 1990; Vlassopoulos *et al.*, 1993).

Rutile is also a useful solid material because of its diverse physical properties and unique photochemical function. The electronic and optical properties of reduced, synthetic rutile and its defect structures have been the subject of a considerable amount of research in the fields of applied physics, solid-state chemistry and materials science (Lu *et al.*, 2001). Rutile, therefore, provides a useful model system for investigating the incorporation of coupled lower-valence cations and hydrogen in NAMs. In addition, the system TiO_2 provides a lower-pressure analogue for understanding the SiO_2 system: rutile is isostructural with stishovite, and investigation of hydroxyl incorporation in rutile could provide useful constraints on the importance of hydroxyl incorporation in stishovite (Smyth *et al.*, 1995).

* E-mail: gbro04@esc.cam.ac.uk
DOI: 10.1180/0026461056930256

Experimental method

Sample synthesis

Several samples of rutile doped with various trivalent and divalent cations were synthesized at 2.0 GPa, 1100ºC under water-saturated conditions to investigate coupled substitution of H and lower-valence cations. Starting mixes were prepared from high-purity oxides: TiO_2 (99.998%), Fe_2O_3 (99.998%), Al_2O_3 (99.99%), Cr_2O_3 (99.999%), Ga_2O_3 (99.99%), MgO (99.99%), and CaO (99.9%). Two series of synthesis experiments were performed. In the first series of experiments, starting mixes of pure TiO_2, and TiO_2 with 1.0, 2.0 and 5.0 wt.% Fe_2O_3 were prepared by weighing out 3 g of the starting mixture, and then grinding the mixture under ethanol in an automated pestle and mortar for at least 2 h. In the second series of experiments, starting mixes were prepared from TiO_2 with 5 wt.% Al_2O_3, Cr_2O_3, Ga_2O_3, MgO and CaO using the same method. Starting mixes for all experiments were loaded into 10 mm long, 5 mm diameter Pt capsules with 10 wt.% water. Capsules were welded shut, placed in pyrophyllite sleeves and loaded into ½ inch talc-pyrex piston-cylinder sample assemblies. These sample assemblies contained an internal, tapered, graphite resistance furnace to ensure minimal temperature gradients along the length of the capsule. Full details of pressure and temperature calibration and accuracy are given in Bromiley and Keppler (2004). Experiments were pressurized to within 90% of the desired run pressure and then heated at 100ºC/min to 1100ºC, before being fully pressurized. Pressure and temperature were continually monitored and maintained throughout the runs. Runs were isobarically quenched by turning off power to the heating circuit whilst maintaining run pressure. Recovered capsules were weighed, pierced and placed in a drying oven, and then reweighed to check for the presence of water. In all experiments water was seen escaping from capsules when pierced.

Sample analysis

Phases were identified by micro-Raman spectroscopy using published spectra for rutile (Goresy *et al.*, 2001) and by powder XRD. Single crystals of all samples were placed on glass slides and spectra obtained using a Dilor labram Raman spectrometer equipped with a 20 mW HeNe laser and a microscope. Compositions of samples were determined by electron microprobe analysis (EMPA). Samples were prepared as grain mounts and analysed using a Cameca SX50 electron microscope operating at 15 kV and 15 nA, using the following standards: $MnTiO_3$ (Ti), gallium arsenide (Ga), chromium metal (Cr), wollastonite (Ca), spinel (Al), enstatite (Mg), hematite (Fe). A count time of 20 s was used for each element.

Infrared spectroscopy

Near-infrared (NIR) spectroscopy was used to investigate hydroxyl incorporation in the synthetic samples. Infrared (IR) spectra were obtained using a Bruker IFS 120 HR high-resolution FTIR spectrometer coupled with a Bruker IR microscope containing all-reflecting Cassegranian optics. The spectrometer contains a permanently aligned Michelson-type interferometer with a 30º angle of incidence on the beam-splitter. Measurements were taken using a tungsten light source, a Si-coated CaF_2 beams-plitter and a narrow-band MCT detector. Up to 400 scans were acquired for each spectrum with a resolution of 1 cm^{-1}. Polarized spectra were recorded using a wire-strip polarizer on a KRS-5 substrate. The optics of the microscope were purged with H_2O- and CO_2-free, purified air during measurements, and the optics of the spectrometer were kept under vacuum to prevent absorption bands caused by water vapour. The FTIR absorption spectra were only obtained from optically clear areas of crystals, using a variable rectangular aperture in the rear focal plane of the 15× Cassegranian objective. Samples were placed on CaF_2 plates and immersed in poly-trichlorofluoroethylene oil to prevent the occurrence of interference fringes. Crystal sizes for samples ranged from 30 to 500 μm, and for some samples, polarized spectra could be obtained from optically aligned crystals. However, for other samples, crystals were too small to be aligned. Therefore, for all samples, water contents were determined using unpolarized radiation. The OH absorption bands in rutile, as in most NAMs, are highly anisotropic, with greatest absorption when the electric vector of the source radiation is polarized perpendicular to the crystallographic *c* axis (Vlassopoulos *et al.*, 1993). Use of unpolarized radiation could, therefore, lead to inaccuracies in calculated water contents. To avoid this possibility, spectra were obtained from a large number of crystals (typically ~20) in each sample,

TABLE 1. Experimental details, results and composition of run products analysed by EMPA.

Sample	Bulk composition	Run products	Colour	Wt.% TiO_2	Wt.% additional oxide	Total
R1	TiO_2	Rutile	Dark blue	–	–	–
RFe1	TiO_2 + 1.0 wt.% Fe_2O_3	Rutile + ilmenite	Dark yellow-brown	99.88(10)	0.21(2)	100.09(21)
RFe2	TiO_2 + 2.0 wt.% Fe_2O_3	Rutile + ilmenite	Yellow-brown	99.72(11)	0.33(3)	100.06(29)
RFe3	TiO_2 + 5 wt.% Fe_2O_3	Rutile + ilmenite	Bright brown	97.22 (56)	2.69(9)	99.91(79)
RAl	TiO_2 + 5 wt.% Al_2O_3	Rutile + corundum	Pale blue	97.93(68)	1.96(15)	99.92(79)
RMg	TiO_2 + 5 wt.% MgO	Rutile + geikielite	Colourless	98.68(32)	0.82(2)	99.50(31)
RCr	TiO_2 + 5 wt.% Cr_2O_3	Rutile	Red-brown	94.42(111)	4.92(82)	99.38(62)
RCr2	TiO_2 + 10 wt.% Cr_2O_3	Carmichaelite (no rutile!)	Dark red-brown	88.90(65)	10.88(42)	99.78(44)
RGa	TiO_2 + 5 wt.% Ga_2O_3	Rutile + unknown phase*	Colourless	96.18(28)	3.92(12)	100.11(28)
RCa	TiO_2 + 5 wt.% CaO	Rutile + $CaTiO_3$ perovskite	Colourless	99.61(11)	0.08(3)	99.69(13)

* XRD pattern of unknown (Ga-Ti oxide?) phase has peaks at *d* spacings of 3.604, 1.87 and 1.81.

and water contents calculated from averaged spectra. Water contents were calculated from integrated IR spectra using the Beer-Lambert law on species absorption, and known IR integral absorption coefficients for rutile. Three different integral absorption coefficients for rutile have been determined: 15,100±500 $Lmol^{-1}cm^{-2}$ (Johnson *et al.*, 1968), 3270 $Lmol^{-1}cm^{-2}$ (Hammer and Beran, 1991) and 38,000 $Lmol^{-1}cm^{-2}$ (Maldener *et al.*, 2001). The large disparities between these values are largely the result of the different techniques used to independently calibrate absorption coefficients and the nature of the samples used for the calibration. In this study, we use the calibration of Johnson *et al.* (1973) because it was derived from a study of synthetic rutile and because it gives calculated water contents for rutile samples closer to values derived using the general sample-independent calibrations of Paterson (1982) and Libowitzky and Rossman (1997).

Fe^{3+} incorporation in synthetic rutile

The compositions of all run products determined by EMPA are listed in Table 1. Water contents calculated from FTIR spectra are listed in Table 2. Samples R1 to RFe3 were synthesized from starting mixtures with Fe_2O_3 contents ranging from 0 to 5 wt.%. Several interesting features are noted from these experiments. Firstly, in all samples containing iron, additional amounts

TABLE 2. H contents (expressed as water contents) for synthetic rutile determined from NIR analysis.

Sample	Integrated absorbance (cm^{-2})	Water content (ppm wt. H_2O)[1]
R1	642	90±3
RFe1	951	134±4
RFe2	2152	302±10
RFe3	6418	900±31
RAl	12671	1777±57
RMg	5470	767±26
RCr	14078	1975±67
RCr2	–	–
RGa	4946	694±23
RCa	0	0

[1] Calculated using the integral absorption coefficients for rutile of Johnson *et al.* (1973). Error on calculated value derived from error for integral absorption coefficient.

of an Fe-rich phase, ilmenite ($FeTiO_3$) are present. Iron was added to starting mixes as hematite (i.e. Fe^{3+}), thereby implying partial reduction of Fe during the experiments. The Fe content of the rutile samples increases with increasing Fe content of the starting mix. Sample RFe3, synthesized from a starting mixture with 5 wt.% Fe_2O_3, has the highest Fe content. The Fe content of this sample is, within error, the same as the sample synthesized under the same *P-T*-H_2O conditions in the study by Bromiley *et al.* (2004a). The only difference in synthesis between these samples is that Bromiley *et al.* (2004*a*) used Pt capsules lined with Re foil to prevent Fe-loss to the capsules during the experiment. No Re lining was used in the present study to minimize differences in f_{O_2} conditions between different experiments. However, comparison of the present results with those of Bromiley *et al.* (2004*a*) suggests that the use of Re foil has an undetectable effect on Fe contents of rutile samples. Iron contents of the samples RFe1 and RFe2 (synthesized from starting mixes with 1.0 and 2.0 wt.% Fe_2O_3, respectively) are considerably lower than sample RFe3 and also much lower than the Fe content of the starting mixes for these experiments. This is an interesting observation because it implies that these samples are under-saturated with respect to Fe. Long run times were used during all experiments to attain chemical equilibrium. During EMPA, no signs of chemical zoning were noted in any rutile samples, and so we assume that the Fe contents of all samples represent equilibrium values.

Another interesting feature of Fe-bearing samples is the colour of the rutile crystals. In sample R1 (Fe-free), rutile crystals are dark blue. This colour is characteristic of rutile samples grown or annealed under reducing conditions. In a detailed spectroscopic study, Khomenko *et al.* (1998) demonstrated that the colour of reduced, TiO_{2-x} rutile is mainly due to intervalence charge transfer (IVCT) between Ti^{3+} and Ti^{4+} on adjacent interstitial and octahedral sites. The IVCT in rutile is evident from broad absorption in the optical to NIR spectral range. This absorption is seen in NIR spectra obtained from rutile as a characteristic broad absorption band centred around 6000 cm^{-1}. Figure 1 shows NIR spectra of samples R1 to RFe3. In contrast to sample R1, sample RFe3 is light yellow in colour. Mössbauer spectra from Fe-doped rutile (Bromiley *et al.*, 2004a) showed that all Fe in synthetic rutile is Fe^{3+}, and demonstrated that Fe^{3+} substitutes for Ti^{4+}; i.e. Fe^{3+} is present on the octahedral Ti^{4+} site. The light colour of rutile in sample RFe3 is, therefore, probably due to electronic transitions in octahedrally co-ordinated Fe^{3+} (Burns, 1993). The NIR spectra obtained from sample RFe3 (Fig. 1) contain no broad absorption bands, implying an absence of Ti^{3+}-Ti^{4+} IVCT. Rutile crystals in samples RFe1 and RFe2 are yellow-brown in colour, implying absorption due to Ti^{3+}-Ti^{4+} IVCT and octahedrally coordinated Fe^{3+}. The NIR spectra from these samples show some absorption around 6000 cm^{-1} (Fig. 1), although markedly less than for sample R1. In fact, there appears to be a marked correlation between Fe content and absorption due to IVCT: increasing Fe content in the synthetic rutile reduces the amount of Ti^{3+}-Ti^{4+} IVCT. A similar phenomenon is well known in industry, where small amounts of trivalent cation substitution (mainly Al^{3+}) in nano-phase rutile is used to suppress optical absorption, giving rutile its desired brilliant white colour. It would appear that at high pressure, Fe^{3+} substitution has a similar effect. This effect can be most easily explained by considering mechanisms for trivalent cation substitution in rutile and the synthesis conditions of rutile samples in the present study. Previous investigations of rutile have demonstrated a number of mechanisms for charge-balancing trivalent cation substitutions (Gesenhues and Rentschler, 1999). In natural rutiles, substitution of trivalent cations can be compensated by substitution of pentavalent cations for Ti^{4+} (e.g. $Fe^{3+} + Nb^{5+} \rightleftharpoons 2Ti^{4+}$). However, in the present study, such mechanisms cannot operate. Alternatively, Fe^{3+} substitution could be charge-balanced by H^+ incorporation. The NIR spectra for samples shown in Fig. 1 contain sharp bands over the OH-stretching range (4000−2500 cm^{-1}), implying the presence of some structurally-incorporated H. However, as can be seen in Tables 1 and 2, H contents of Fe-doped rutile are several orders of magnitude lower than Fe contents, implying that another mechanism is needed to compensate most of the Fe substitution in the samples. Alternatively, Fe substitution could either be charge-balanced by the coupled substitution of trivalent cations (either Fe^{3+} or Ti^{3+}) onto interstitial sites or by oxygen vacancies. A wealth of information is available on defects present in reduced rutile (Lu *et al.*, 2001), and there is abundant evidence indicating that both oxygen vacancies and Ti intersitials are present as stable defects. The experimental setup

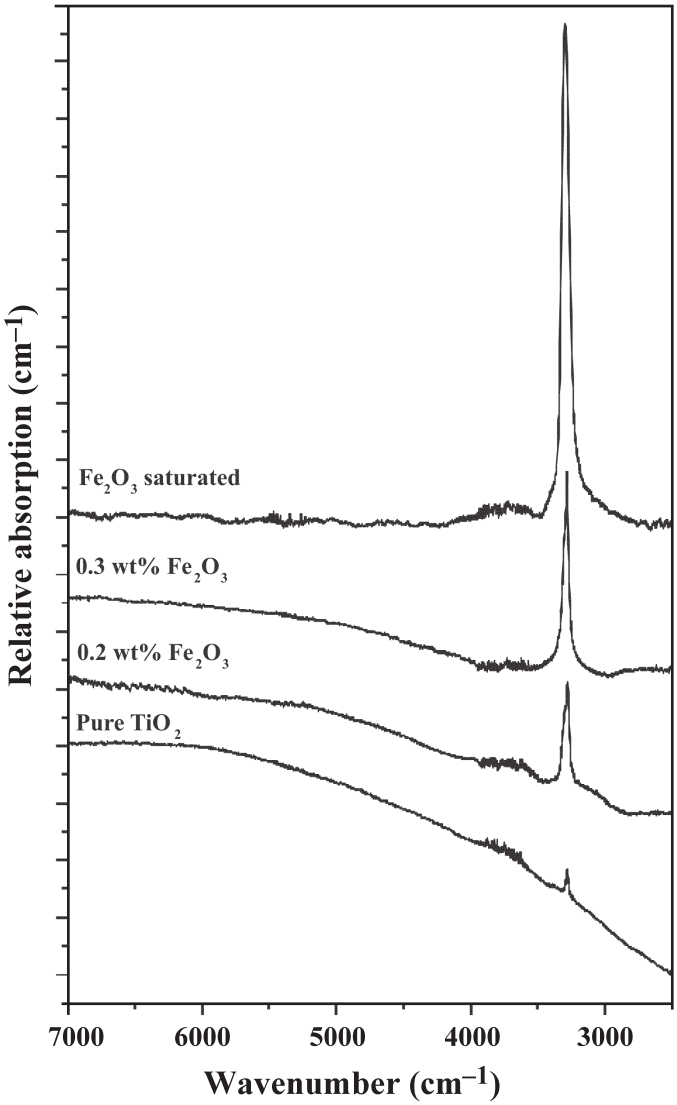

FIG. 1. NIR spectra of rutile doped with increasing amounts of Fe_2O_3 synthesized under water-saturated conditions at 2.0 GPa, 1100ºC. A horizontal baseline over the spectral range shown has been subtracted. Spectra offset vertically with increasing Fe content for clarity. Large and small divisions on the vertical scale represent 10 and 5 cm^{-1}, respectively.

used in this study produces slightly reducing conditions for sample synthesis (presumably due to the large graphite furnace used in the run assembly). Oxygen fugacity for the experimental setup is estimated to be slightly lower than NNO (Bromiley *et al.*, 2004*b*), as long as reaction of the starting materials has only a limited influence. Fe substitution in rutile charge-balanced by oxygen vacancies would, therefore, appear possible. Bromiley *et al.* (2004*a*) suggested that this was the most likely mechanism for charge-balancing Fe incorporation in rutile and its high-pressure form TiO_2 (II) because Mössbauer spectra from both phases consisted of a single quadrupole doublet (due to octahedrally-coordinated Fe^{3+}), with no evidence noted for Fe^{3+} occupancy of more than one site. This observation is important, because although the main interstitial site in rutile

is octahedral, it is considerably more distorted than the regular Ti^{4+} site, and occupancy of both octahedral and interstitial sites by Fe^{3+} should be detectable by Mössbauer spectroscopy. However, this would not completely exclude the possibility that a small amount of Fe^{3+} in the synthetic rutile could also be present on the main interstitial site. Interstitial Ti^{3+} in samples RFe1 and RFe2 could provide an additional charge-balancing mechanism for Fe substitution. However, this is a somewhat unsatisfactory conclusion to draw because it does not fully explain why there is no interstitial Ti^{3+} in sample R3, and is inconsistent with the observed decrease in IVCT absorption with increasing Fe content. To explain some of the unusual features noted in these experiments, we need first to summarize what we know about stable defects present in the reduced rutile samples, and what reactions must occur during the synthesis of Fe-bearing rutile.

Firstly, it has been demonstrated that reduced rutile (pure TiO_2) contains interstitial Ti^{3+} ($Ti_i^{\cdots}$ in the Kröger-Vink notation), presumably some octahedral Ti^{3+} ($Ti_{Ti}^{/}$) and oxygen vacancies ($V_O^{\cdots}$) as stable defects. For the present discussion we will ignore the minor effect that H interstitials ($H_i^{\cdot}$) could have. In the Fe-doped samples we also have $Fe_{Ti}^{/}$ defects and possibly small amounts of interstitial Fe ($Fe_i^{\cdots}$). $Ti_i^{\cdots}$ are only present in samples RFe1 and RFe2, which also have lower Fe contents than might be expected. If we conclude that the main mechanism for charge-balancing $Fe_{Ti}^{/}$ are $V_O^{\cdot\cdot}$ (as decoupled defects, because Fe is in octahedral coordination), then we can assume that the Fe content of Fe-saturated rutile is a function of f_{O_2}. Therefore, the reducing conditions of the experimental synthesis would effectively govern the amount of Fe^{3+} incorporated. However, in the different synthesis experiments, several competing reactions must occur, and these probably affect f_{O_2} in turn. Presumably, Fe_2O_3 in the starting mixture reacts with TiO_2 to form Fe-doped rutile, but must also be partly reduced and react with TiO_2 to form ilmenite. We can write a simple equation to describe the equilibrium condition:

$$\underset{\text{ilmenite}}{2FeTiO_3} + \tfrac{1}{2}O_2 = \underset{\text{rutile}_{ss}}{Fe_2O_3} + \underset{\text{rutile}_{ss}}{2TiO_2} \qquad (1)$$

where ss indicates solid solution of the components in rutile. In Fe-rich systems, reaction 1 probably controls the f_{O_2} in the capsule, buffering it to a higher value than expected. In contrast, experiments performed using low bulk Fe_2O_3 contents must be more reducing, because the presence of $Ti_i^{\cdots}$ defects in Fe-poor rutile implies TiO_2 reduction. According to reaction 1, more reducing conditions would result in lower Fe_2O_3 contents in rutile, which is exactly what is seen in our experiments. This situation is probably further complicated by the additional, minor effect of H incorporation in rutile, which implies breakdown of H_2O. However, the overall effect of bulk Fe_2O_3 content on the Fe_2O_3 content of rutile and the concentration of $Ti_i^{\cdots}$ defects in rutile strongly suggests that the controlling factor in all experiments is the f_{O_2}, which can be buffered at higher values in Fe-rich systems relative to Fe-poor systems, because Fe_2O_3 in the starting mix acts as a source for O_2. In turn, this implies that Fe^{3+} substitution for Ti^{4+} in rutile is mainly charge-balanced by $V_O^{\cdot\cdot}$ rather than by interstitial cations. Unfortunately, Fe_2O_3 contents of samples RFe1 and RFe2 were too low for investigation of Fe incorporation using Mössbauer spectroscopy, which might reveal any differences in mechanisms for Fe incorporation between samples RFe1 and RFe2 compared to RFe3. Further attempts to synthesize Fe-undersaturated rutile with Fe contents >0.3 wt.% using various additional solid oxygen buffers have been unsuccessful, probably due to the dominant influence of the bulk composition on prevailing oxygen fugacity during synthesis.

H incorporation in rutile as a function of Fe_2O_3 content

As previously noted, all NIR spectra shown in Fig. 1 contain sharp OH-absorption bands, implying the presence of structurally-incorporated H. These OH-absorption bands are shown in more detail in Fig. 2. Spectra obtained from R1 (pure TiO_2) contain one absorption band at 3279 cm^{-1}, implying the presence of H in one position in the rutile structure. Due to the absence of other substitutional impurities, H incorporation in R1 is probably charge-balanced by Ti^{3+} reduction. Swope *et al.* (1995) refined the H position in a natural, H-bearing rutile from neutron diffraction data, and demonstrated that H is incorporated in rutile close to (½½0), just off the shared O-O edge in the octahedral chain. This assignment is consistent with published polarized IR spectra from synthetic and natural rutile (Johnson *et al.*, 1968; Vlassopoulos *et al.*, 1993), where vibration of the OH dipole is almost completely perpendicular to the crystallographic *c* axis. In contrast to

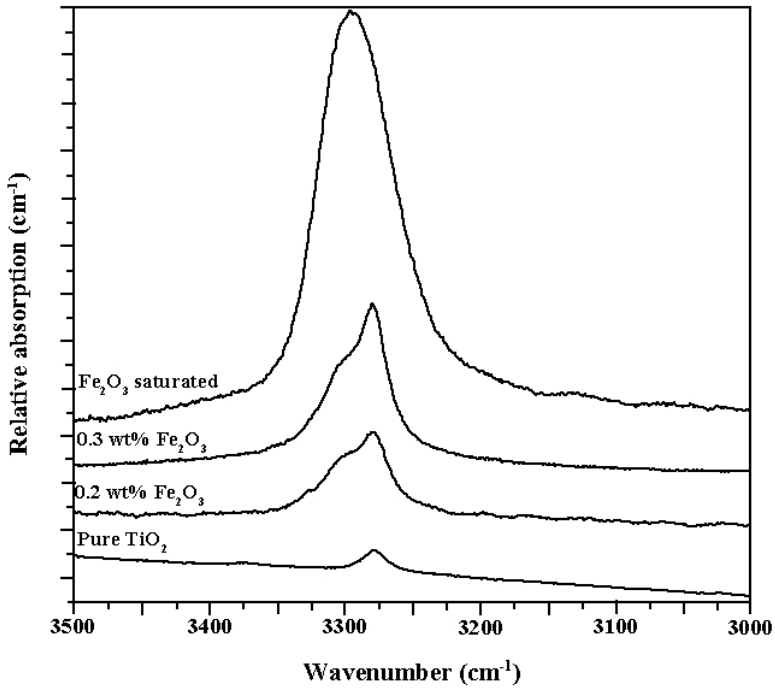

FIG. 2. OH-stretching region of the NIR spectra shown in Fig. 1 (vertical offset rescaled). Large and small divisions on the vertical scale represent 10 and 5 cm^{-1}, respectively.

the R1 spectrum shown in Fig. 2, IR spectra obtained from synthetic, high-pressure water-saturated rutile by Khomenko *et al.* (1998) contain two OH-absorption bands, a large band at 3279 cm^{-1} (i.e. similar to the band in the spectrum from R1), and a smaller, additional band at 3324 cm^{-1}. This second absorption band has also been noted in some other studies of synthetic rutile (e.g. Hammer and Beran, 1991) and shows the same anisotropy as noted for the band at 3279 cm^{-1}. Based on the behaviour of these two bands during annealing, Khomenko *et al.* (1998) suggested that the band at 3324 cm^{-1} was due to H related to Ti^{3+} (i.e. $Ti_{Ti}^{/}$), whilst the band at 3379 cm^{-1} was due to H unrelated to any Ti^{3+} defects. This assignment is in accordance with spectroscopic investigation of natural rutile (Johnson *et al.*, 1968; Vlassopoulos *et al.*, 1993); IR spectra of natural rutiles often contain a sharp absorption band at 3279 cm^{-1}, and more rarely, additional absorption bands at higher or lower wavenumbers. Johnson *et al.* (1968) suggested that the band at 3279 cm^{-1} was due to H not associated with any compositional defects, and that other OH bands were due to H associated with trivalent or divalent cations on the Ti^{4+} octahedral site. If correct, this assignment implies that all the H present in sample R1 is decoupled from any Ti^{3+} defects.

Spectra obtained from rutile in samples R1 and R2 contain two overlapping absorption bands, one at 3279 cm^{-1} (similar to R1) and an additional band at 3295 cm^{-1}. This additional band is probably due to H associated with Fe^{3+} impurities. Regardless of whether we assign the OH band at 3279 cm^{-1} to H associated with Ti^{3+} or H unassociated with compositional impurities, the shift of the additional (3295 cm^{-1}) OH band to lower wavenumbers strongly implies NNN effects. That is, H and Fe^{3+} probably form a defect cluster, with the proton associated with an O surrounding a Ti octahedral site occupied by Fe^{3+} (i.e. $Fe_{Ti}^{/} - H_i^{\cdot}$). From this we can conclude that in the Fe-doped samples, a certain amount of structurally incorporated H becomes coupled to $Fe_{Ti}^{/}$ defects, with the remaining H either decoupled, or conceivably coupled with $Ti_{Ti}^{/}$ defects. Spectra obtained from sample R3 also contain the $Fe_{Ti}^{/} - H_i^{\cdot}$ absorption band at 3295 cm^{-1}. In the R3 spectrum in Fig. 2 this

band is broad and appears to be slightly asymmetric. By comparing all the spectra in Fig. 2, it can be seen that the 3295 cm^{-1} band in this spectrum probably contains a shoulder at 3279 cm^{-1}, implying the presence of H not associated with $Fe_{Ti}^{/}$, or H associated with $Ti_{Ti}^{/}$. In the first instance this would imply that even in Fe-rich rutile, a considerable proportion of the H remains decoupled from substitutional impurities, which could have an important influence on H mobility and H diffusion in rutile. In the second instance, the presence of an additional band would imply the presence of reduced Ti only on octahedral sites and not on interstitial sites (i.e. no absorption due to IVCT) in the Fe-rich sample, and would imply that H solubility in the Fe-rich rutile sample is too great only to be compensated by $Fe_{Ti}^{/}$ defects. This last conclusion is somewhat problematic, because the Fe^{3+} content of this sample is several orders of magnitude higher than the H content, implying that isolated $Fe_{Ti}^{/}$ defects (which must be decoupled from $V_O^{\cdot\cdot}$ due to evidence from Mössbauer spectroscopy) are intrinsically more stable than coupled $Fe_{Ti}^{/} - H_i^{\cdot}$ defects.

One striking feature of the spectra shown in Fig. 2 is that the height of all OH absorption bands increases significantly with increasing Fe content of the samples. This implies that water contents of the samples increase with increasing Fe content. Lower water contents in Fe-poor samples are probably related to the presence of interstitial Ti^{3+}, which could quite conceivably reduce H affinity in the samples due to an increase in O overbonding. It should be noted that increasing H contents with Fe content do not reflect the relative H affinity of rutile due to differences between the H incorporation mechanisms (i.e. $Fe_{Ti}^{/} - H_i^{\cdot}$ compared to $H_i^{\cdot}$ or $Ti_{Ti}^{/} - H_i^{\cdot}$) because both the bands at 3279 and 3295 cm^{-1} show an increase in peak height with increasing Fe content.

Solubility of minor elements in synthetic rutile

Experimental details, run products and the compositions of rutile are listed in Table 1. In all experiments except RCr2, rutile was the main run product. In all experiments except R1 (pure TiO_2) and RCr, small amounts of an additional phase were also present, implying saturation of the rutile with respect to the additional oxides. In experiment RCr, no additional phase was present, and the rutile contains, within error, the same amount of Cr_2O_3 as the starting mixture, possibly implying undersaturation. To determine whether this was the case, we performed an additional experiment, RCr2, using a starting mixture with 10 wt.% Cr_2O_3. In this experiment, the phase carmichaelite was synthesized, and no rutile was present in the run products. Carmichaelite, $[MO_{2-x}(OH)_x$, where M includes Ti, Cr, Fe, Mg and Al] is a hydrous titanate only recently described (Wang *et al.*, 1999; Wang *et al.*, 2000). Wang *et al.* (2000) describe an occurrence of carmichaelite in Garnet Ridge, Arizona, where it precipitated with its pyrope host and other titanates at temperatures of 650–750ºC, and pressures of 2.0–2.5 GPa. They concluded that carmichaelite is probably stabilized by high pressure and high Cr contents. This appears to be consistent with the results of experiments RCr and RCr2, with carmichaelite only stabilized with Cr contents above 5 wt.%. The temperature of synthesis of experiment RCr2 demonstrates a high thermal stability for this phase. To our knowledge, this is the only reported synthesis of this phase, and more work is required to determine its stability and possible significance for mantle geochemistry.

From Table 1 it can be seen that the solubility of additional oxides in the rutile samples varies considerably as a function of composition. For Fe-bearing samples a complex relationship between bulk composition and f_{O_2} appears to have an effect on Fe_2O_3 solubility in the samples. However, this situation is not expected to be as complex for Al^{3+}, Mg^{2+}, Cr^{3+}, Ga^{3+}, Ca^{2+} because these cations only have one common oxidation state in rock-forming minerals (except Cr, which may be present as Cr^{2+} under exceptional circumstances). The NIR spectra from all rutile samples except R1, RFe1 and RFe2 show no broad absorption bands due to Ti^{3+}-Ti^{4+} IVCT. However, in sample RAl, rutile crystals are very pale blue. The colour of these crystals cannot be due to a crystal field effect involving Al^{3+} substitution because it has no electrons in d orbitals. More likely, this slight colouration is also due to Ti^{3+}-Ti^{4+} IVCT, presumably below the detection limit of the spectrometer. Likewise, Ga-, Ca- and Mg-bearing rutile crystals are colourless due to a complete absence of Ti^{3+}. In contrast, Cr-bearing rutile is dark red-brown, probably due to a crystal field splitting effect involving Cr^{3+} on a cation site (Burns, 1993), presumably $Cr_{Ti}^{/}$.

Figure 3 shows a plot of difference in ionic radii between various cations from that of Ti^{4+}

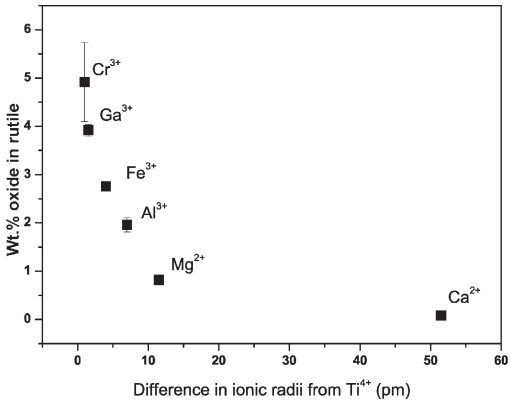

FIG. 3. Plot of difference in ionic radius (6-coordinated, octahedral sites) between cations used as additional oxides in the present study and Ti^{4+} against solubility of oxides in the synthetic, water-saturated rutile at 2.0 GPa, 1100ºC. Values of ionic radius are listed in Table 2.

against their measured solubility in synthetic rutile. A clear trend is noted in the plot. With increasing difference in ionic radii, the solubility of the cation decreases. Such a relationship would be expected for direct substitution of various cations for Ti^{4+}. However, this plot masks some obvious discrepancies. Firstly, we have seen that Fe_2O_3 reduction probably has an influence on solubility of Fe_2O_3 in rutile in sample RFe3. Secondly, sample RCr is possibly Cr-undersaturated, although, by inference to the Fe-bearing series of experiments, the lack of IVCT may indicate that rutile in this sample is close to, or at, saturation. Thirdly, and to a lesser degree, we can infer that in addition to Al^{3+}, sample RAl also contains Ti^{3+} defects. However, the broad trend that we see in Fig. 3 probably indicates a similar incorporation mechanism for the various trivalent and divalent cations in rutile. As noted above, Mössbauer spectra obtained from Fe-doped rutile and TiO_2(II) indicate that Fe^{3+} in both phases is present on the octahedral (Ti^{4+}) site (Bromiley *et al.*, 2004*a*). Computer simulations of defect structures in rutile have also demonstrated that Cr^{3+}, Al^{3+}, Ga^{3+} and Fe^{3+} are preferentially incorporated in rutile onto the octahedral site, charge-balanced by oxygen vacancies (Sayle *et al.*, 1995). In a study of synthetic Al-doped rutile, Gesenhues and Rentschler (1999) showed that at ambient pressure, Al^{3+} substitution for Ti^{4+} is charge-balanced by oxygen vacancies, but that with increasing Al_2O_3 contents, some Al^{3+} is additionally put onto interstitial sites. However, the most important mechanism for incorporation of lower-valence cations in synthetic rutile is probably direct substitution for Ti^{4+} (i.e. direct substitution onto the octahedral site in the rutile structure), charge-balanced by proton incorporation or oxygen vacancies. It is possible that to a much lesser degree trivalent cations are also present on interstitial sites. Lack of a noticeable deviation for Fe^{3+} from the trend in Fig. 3 could imply that any change in Fe_2O_3 solubility due to self-buffering of f_{O_2} is not large enough to be detected. Likewise, the presence of $Ti_i^{\cdot}$ in rutile in sample RAl does not alter Al solubility by a large enough degree to influence the plot in Fig. 3. However, it is possible that with extension of the present dataset to include the solubility of a larger number of trivalent and divalent cations in rutile, such deviations could be observed.

Coupled H and minor element incorporation in synthetic rutile

The NIR spectra obtained from synthetic rutile doped with 5 wt.% additional oxides are shown in Fig. 4. All spectra, except those obtained from sample RCa (not shown), contain OH-stretching absorption bands over the wavenumber range 4000–2500 cm^{-1}, implying the presence of structurally-incorporated H. Spectra obtained from RCa1 contained no features over this wavenumber range, implying an absence of H in the structure. Polarized spectra were obtained from crystals in samples RFe, RCr and RGa, and show that the main absorption bands in these spectra have a 95% component of vibration perpendicular to the crystallographic *c* axis, consistent with the H incorporation mechanism proposed by Swope *et al.* (1995). The water contents for all samples were calculated from unpolarized IR spectra and are listed in Table 2.

Spectra from all samples consist of one main absorption band. In Fe-, Al-, Cr- and Ga-bearing rutile, this absorption band is at 3295, 3308, 3257 and 3314 cm^{-1}, respectively. Variation in the wavenumber of the main OH band with composition is consistent with the formation of coupled defects involving trivalent cations and H, ($M_{Ti}^{/} - H_i^{\cdot}$). In addition to the main OH-absorption band, these spectra also contain an additional band at ~3279 cm^{-1}, usually only seen as a slight shoulder on the main OH-absorption band. As noted for the Fe-bearing samples, this band is probably due to H decoupled from any

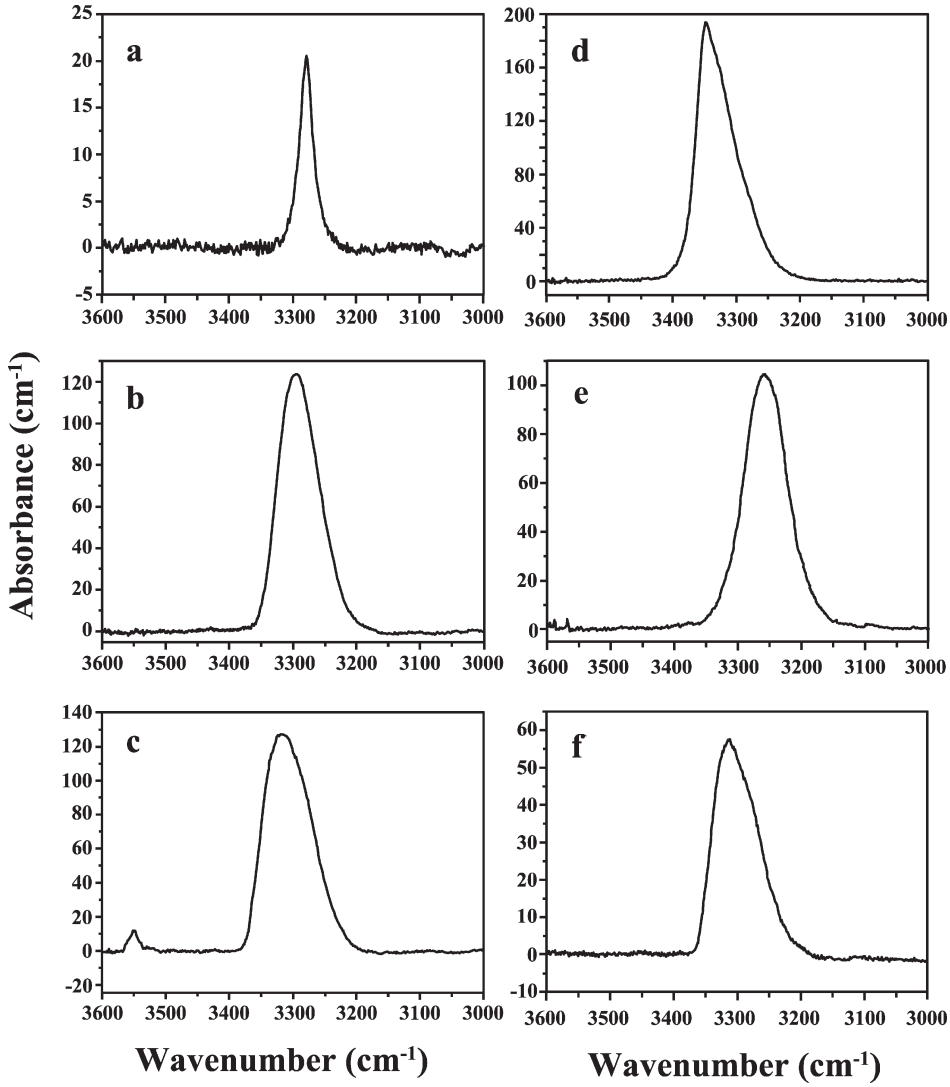

FIG. 4. Unpolarized average NIR spectra (over the OH-stretching range) from synthetic, water-saturated rutile grown at 2.0 GPa, 1100ºC. (*a*) R1, (*b*) RFe3, (*c*) RAl, (*d*) RMg, (*e*) RCr, (*f*) RGa.

compositional defects, but could also be due to H associated with Ti^{3+}. Spectra from sample RAl also contain a small OH absorption band at much higher wavenumbers, 3551 cm^{-1}, which is not seen in the spectra of any other samples, and suggests that there is another mechanism for H incorporation in the Al-bearing rutile. Gesenhues and Rentschler (1999) noted that synthetic rutile grown at ambient pressure doped with large amounts of Al_2O_3 contains Al^{3+} on both octahedral and interstitial sites. The additional band at 3551 cm^{-1} could possibly be due to H^+ incorporation related to interstitial Al^{3+}. Unfortunately no data are available on the anisotropic nature of this small band, so direct assignment is not possible. However, several potential positions for H incorporation in the rutile structure have been identified (Johnson *et al.*, 1968), and the band at 3551 cm^{-1} could be due to H^+ in a ½00 position.

Spectra obtained from Mg-bearing rutile contain an asymmetric band at 3349 cm^{-1}, which can actually be resolved into three separate bands, a large band at 3349 cm^{-1}, a shoulder at

3325 cm^{-1} and another small band at 3279 cm^{-1} (i.e. the OH band noted in all spectra). This interpretation implies that there are two H positions associated with Mg^{2+}, one slightly more favourable. The OH-stretching frequencies of these two absorption bands are similar, and no variation in relative peak height was noted as a function of orientation, implying no distinct difference in absorption band anisotropy. The H incorporation mechanism proposed by Swope *et al.* (1995) actually describes four equivalent H positions about a symmetrical, regular octahedron. Local distortion of the octahedral site in rutile due to Mg^{2+} substitution could potentially result in slight differences in OH-stretching frequencies for H^+ located in these different positions. If H incorporation in the MgO-saturated rutile is related to Mg substutition for Ti^{4+}, this would imply that two H^+ are incorporated for every Mg^{2+}. Differences in the peak height of the absorption bands could indicate that, as a result of site distortion, the four equivalent H positions are split into at least two pairs with slightly differing OH-stretching frequencies, with the slightly longer O−H bond being more favourable.

It is interesting to note, on the basis of absorption-band assignment, that IR spectra obtained from Ca-doped rutile (RCa) contain no OH absorption bands. This implies that H incorporation coupled with $Ca_{Ti}^{//}$ is not stable. Indeed, decoupled H interstitials, or H interstitials coupled with Ti^{3+} defects are also not present in this sample. As noted in Table 3, the difference in ionic radii between Ti^{4+} and Ca^{2+} is quite high (51.5 pm). Lack of structurally incorporated H in sample RCa could be due to considerable distortion of the Ti site in the rutile structure due to Ca occupancy. However, this does not sufficiently explain the absence of the 3279 cm^{-1} band. This could indicate that a significant amount of Ca^{2+}, in contrast to the other trivalent and divalent cations considered, occupies interstitial sites in the rutile structure. From Figs 1 and 2 it can be seen that the presence of interstitial Ti markedly reduces the affinity of rutile for H. Perhaps a similar effect is noted in the Ca-doped sample due to interstitial Ca. The presence of $Ca_i^{\cdot\cdot}$ defects could be charge-balanced by the coupled substitution of Ca onto the octahedral Ti site ($Ca_{Ti}^{//}$) or by reduction of Ti^{4+} ($Ti_{Ti}^{/}$). The absence of broad absorption bands in NIR spectra from RCa over the range 700 to 4000 cm^{-1}, or indeed of any blue colouration of the Ca-doped crystals, excludes the possibility of Ti^{3+} interstitials being present, but not of reduced Ti^{4+} on the main Ti site. The use of Ca-doping of rutile to prevent H incorporation could, potentially, have some important industrial applications.

TABLE 3. Ionic radii of cations in 6-coordinated octahedral environments.

Cation	Ionic radius (pm)
Ti^{4+}	74.5
Fe^{3+}	78.4
Al^{3+}	67.5
Mg^{2+}	86.0
Ga^{3+}	76.0
Cr^{3+}	75.5
Ca^{2+}	126.0

An interesting feature in IR spectra obtained from the synthetic rutile samples is the significant variation in the width of the OH absorption bands as a function of composition. Mostly, this effect is due to overlapping of the main OH absorption band, which has a different frequency in each composition, with the smaller absorption band at 3279 cm^{-1}. However, there could also be some variation in the width of the main absorption band as a function of composition, possibly due to NNN effects: the presence of small amounts of interstitial trivalent cations, or, in the example of RCr, increased likelihood of trivalent cations being on adjacent octahedral (Ti^{4+}) sites due to higher solubility of the minor element. Significant variation in water solubility in the synthetic rutile is also noted as a function of composition. The highest water content measured is for the Cr-doped sample. However, no systematic variation in water content as a function of oxide solubility or ionic radius is seen. Water solubility probably varies partly as a function of the change in unit-cell volume due to H incorporation, and should, therefore, be partly dependent upon relative distortion due to $M_{Ti}^{/}$ defects. However, we have seen that in all samples some H is also present which is either decoupled to compositional defects, or related to the presence of Ti^{3+}. Furthermore, at least one of the samples, RAl, contains cations on interstitial sites, which probably leads to a reduction in H solubility. Unfortunately, it is not possible to determine accurately the areas of overlapping absorption bands in the IR spectra, and therefore the amount of H coupled to (or decoupled from) different defects. Peak fitting is made difficult by the fact

that: (1) the signal to noise ratio is not ideal, mainly due to the small sample size and low concentration of H, (2) most absorption bands are broad and the amount of overlap is large, and (3) background subtraction can lead to changes in relative peak heights. Calculated water contents may not, however, be directly comparable anyway, because of variation in OH-stretching frequencies as a function of composition. Nakamoto *et al.* (1955) noted that there is a significant dependence of H concentration on OH-stretching frequency, which would imply a systematic overestimation of water contents in samples where the main OH absorption band is shifted to higher wavenumbers.

Comparison with natural samples

Johnson *et al.* (1968) first suggested that H incorporation in rutile was linked to trivalent cation substitutions, but they were not able to resolve impurity-associated OH bands in IR spectra from rutiles doped with various oxides and so concluded that either there was no association of OH groups with cations, or that resulting shifts in OH-stretching bands were too small to be resolved. However, in detailed investigations of coupled H and minor element substitution in natural rutiles from various geological terrains, Hammer and Beran (1991) and Vlassopoulos *et al.* (1993) noted systematic shifts in OH-stretching frequencies, and attempted to correlate these with variation in composition and geological environment. Spectra obtained from many natural rutiles commonly contain one main absorption band at 3280 to 3390 cm^{-1} (e.g. samples R-6, R-7, R-8, JAG83-30-3, JAG85-2 of Vlassopoulos *et al.*, 1993). Fe^{3+} is the major trivalent cation in many natural rutiles. Spectra from the synthetic Fe-saturated rutile, RFe3, contain an absorption band at 3295 cm^{-1}, which may be comparable to the band seen in spectra from natural rutiles. Samples R-6 to R-8 of Vlassopoulos *et al.* (1993) contain appreciable amounts of Fe. In contrast, samples JAG83-30-3 and JAG85-2 contain much larger amounts of Cr. Spectra from sample RCr contain an absorption band at significantly lower wavenumbers (3257 cm^{-1}), and are not comparable to spectra obtained from these natural Cr-rich rutiles. An alternative explanation is that the main absorption band in IR spectra from natural rutiles is unrelated to compositional impurities, and is comparable to the band at 3279 cm^{-1} seen in all IR spectra from synthetic rutile in the present study. This explanation appears to be more consistent with the similarities between IR spectra obtained from natural rutile samples with different compositions. Furthermore, this assertion supports the argument that the 3279 cm^{-1} OH-absorption band seen in spectra in Figs 2 and 4 is due to H unrelated to compositional impurities, because natural rutiles only contain Ti^{3+} under extremely limiting circumstances, such as in meteoritic or lunar samples for which oxygen fugacity during crystallization was extremely low.

Vlassopoulos *et al.* (1993) noted that rutiles from mafic pegmatites contained an additional absorption band around 3360 cm^{-1}, and suggested that this may be due to H association with Mg^{2+}. This correlates reasonably well with data from the present study, where Mg-saturated rutiles contain a large absorption band at 3349 cm^{-1}. However, Vlassopoulos *et al.* (1993) also suggest that a small satellite peak at 3324 cm^{-1} seen in some rutile spectra, is due to association with Al^{3+}. This suggestion is not consistent with the results of the present study.

Spectra obtained from synthetic rutile samples doped with various trivalent and divalent cations replicate many of the features seen in spectra of natural samples. Vlassopoulos *et al.* (1993) measured integrated absorbances over the OH-stretching range in spectra from natural samples from 1800 to 12300 cm^{-2}. Values obtained from the synthetic samples in this study range from 640 cm^{-2} (for pure TiO_2) to 14100 cm^{-2}. The largest values measured by Vlassopoulos *et al.* (1993) were for rutiles from ultra-high pressure environments, and are in very good agreement with data from our study. Interestingly, the greatest water content noted by Vlassopoulos *et al.* (1993) was for a Cr-rich sample, and the greatest water content of any sample in this study was measured for the Cr-doped sample. However, results from the present study indicate that many of the correlations between OH-stretching frequencies and compositions previously reported are overstated. Most likely, a significant proportion of H in natural rutiles is not coupled to substitutional impurities. If so, this implies that small variations in OH-stretching frequencies between different rutile samples is probably due to some variation in the size and/or distortion of the octahedral (Ti^{4+}) site in the structure, which should be evident from detailed structural refinements. Furthermore, H incorporation in natural rutiles could be linked to

Ti^{4+} substitution for pentavalent cations on octahedral sites in the rutile structure. Natural rutiles often contain appreciable Nb and Ta, and so this could provide an efficient mechanism for H incorporation, and would also result in the formation of H interstitials unrelated to other compositional impurities.

Defect structures in synthetic and natural rutile

The main mechanism for H incorporation in the synthetic rutile samples is association with lower-valence cation substitution onto octahedral sites. However, the amount of water incorporated into rutile (Table 3) is at least one order of magnitude lower than the solubility of lower-valence cations (Table 1), implying that the dominant mechanism for trivalent and divalent cation substitution into the synthetic rutile does not involve H incorporation. We have argued that the dominant mechanism for trivalent and divalent cation substitution in synthetic rutile probably involves oxygen vacancies, and to a lesser degree, could also involve cations on interstitial sites. In natural rutile, trivalent cation substitutions can also be charge-balanced by coupled substitutions with pentavalent cations (i.e. $M^{3+} + M^{5+} = 2\ Ti^{4+}$). The extent to which natural high-pressure rutiles are reduced, and the extent to which oxygen vacancies can charge-balance trivalent cation substitutions is not known. However, redox conditions in the piston-cylinder assembly probably closely resemble redox conditions expected in many geological environments where rutile is an important accessory mineral, such as subducting slabs (Bromiley *et al.*, 2004*b*). Vlassopoulos *et al.* (1993) noted that the total trivalent cation content of a suite of rutile samples was systematically higher than the total pentavalent cation content, and suggested that this was due to large amounts of H incorporation. The amount of H needed to charge balance the excess trivalent cation content in many rutiles is considerable, and has been used as an argument in favour of using the integral absorption coefficient determined by Hammer and Beran (1991), which gives unrealistically high water contents. However, the presence of oxygen vacancies in natural rutile, or the presence of interstitial cations could also account for a large amount of excess trivalent cation content, and would imply that the Hammer and Beran (1991) calibration significantly overestimates the water content of rutile relative to the calibration of Johnson *et al.* (1973) and the sample independent calibrations of Paterson (1982) and Libowitzky (1999).

Acknowledgements

The authors would like to thank Heinz Fischer, Georg Herrmannsdörfer, Detlef Krauße and Hubert Schulze for technical assistance, and Fabrice Gaillard and Fiona Bromiley for help with preparation of the manuscript. This manuscript was improved by the comments of an anonymous reviewer.

References

Bromiley, G. and Keppler, H. (2004) An experimental investigation of hydroxyl solubility in jadeite and Na-rich pyroxenes. *Contributions to Mineralogy and Petrology*, **147**, 189–200.

Bromiley, G., Hilairet, N. and McCammon, C. (2004*a*) Solubility of hydrogen and ferric iron in rutile and TiO_2 (II): Implications for phase assemblages during ultrahigh-pressure metamorphism and for the stability of silica polymorphs in the lower mantle. *Geophysical Research Letters*, **31**, L04610.

Bromiley, G., Keppler, H., McCammon, C., Bromiley, F. and Jacobsen, S. (2004*b*) Hydrogen solubility and speciation in natural, gem-quality Cr-diopside. *American Mineralogist*, **89**, 941–949.

Burns, R. (1993) *Mineralogical Applications of Crystal Field Theory*. Cambridge University Press, Cambridge, UK, 551 pp.

Deer, W., Howie, R.A. and Zussman, J. (1992) *An Introduction to the Rock-Forming Minerals*. Longmans, Essex, UK, 696 pp.

Gesenhues, U. and Rentschler, T. (1999) Crystal growth and defect structure of Al^{3+}-doped rutile. *Journal of Solid State Chemistry*, **143**, 210–218.

Goresy, A., Chen, M., Gillet, P., Dubrovinsky, L., Graup, G. and Ahuja, R. (2001) A natural shock-induced dense polymorph of rutile with alpha-PbO_2 structure in the suevite from the Ries crater in Germany. *Earth and Planetary Science Letters*, **192**, 485–495.

Hammer, V. and Beran, A. (1991) Variations in the OH concentrations of rutile from different geological environments. *Mineralogy and Petrology*, **45**, 1–9.

Johnson, O., Ohlsen, W. and Kingsbury, P., Jr. (1968) Defects in rutile (iii). Optical and electrical properties of impurities and charge carriers. *Physical Review*, **175**, 1102–1108.

Johnson, O., DeFord, J. and Shaner, J. (1973) Experimental technique for the precise determination of H and D concentration in rutile (TiO_2). *Journal of*

Applied Physics, **44**, 3008–3012.

Khomenko, V., Langer, K., Rager, H. and Fett, A. (1998) Electronic absorption by Ti^{3+} ions and electronic delocalization in synthetic blue rutile. *Physics and Chemistry of Minerals*, **25**, 338–346.

Libowitzky, E. (1999) Correlation of O-H stretching frequencies and O-H···O hydrogen bond lengths in minerals. *Monatshefte für Chemie*, **130**, 1047–1059.

Libowitzky, E. and Rossman, G. (1997) An IR absorption calibration for water in minerals. *American Mineralogist*, **82**, 1111–1115.

Lu, T.-C., Wu, S.-Y., Lin, L.-B. and Zheng, W.-C. (2001) Defects in the reduced rutile single crystal. *Physica B*, **304**, 147–151.

Maldener, J., Rauch, F., Gavranic, M. and Beran, A. (2001) OH absorption coefficients of rutile and cassiterite deduced from nuclear reaction analysis and FTIR spectroscopy. *Mineralogy and Petrology*, **71**, 21–29.

Nakamoto, K., Margoshes, M. and Rundle, R. (1955) Stretching frequencies as a function of distances in hydrogen bonds. *Journal of the American Chemical Society*, **77**, 6480–6486.

Paterson, M. (1982) The determination of hydroxyl by infrared absorption in quartz, silicate glasses and similar materials. *Bulletin of Mineralogy*, **105**, 20–29.

Rossman, G. and Smyth, J. (1990) Hydroxyl contents of accessory minerals in mantle eclogites and related rocks. *American Mineralogist*, **75**, 775–780.

Sayle, D., Catlow, C., Perrin, M.-A. and Nortier, P. (1995) Computer simulation study of the defect chemistry of rutile TiO_2. *Journal of the Physics and Chemistry of Solids*, **56**, 799–805.

Smyth, J., Swope, R. and Pawley, A. (1995) H in rutile-type compounds: II. Crystal chemistry of Al substitution in H-bearing stishovite. *American Mineralogist*, **80**, 454–456.

Swope, R., Smyth, J. and Larson, A. (1995) H in rutile compounds: I. Single-crystal neutron and X-ray diffraction study of H in rutile. *American Mineralogist*, **80**, 448–453.

Vlassopoulos, D., Rossman, G. and Haggerty, S. (1993) Coupled substitution of H and minor elements in rutile and the implications of high OH contents in Nb- and Cr-rich rutile from the upper mantle. *American Mineralogist*, **78**, 1181–1191.

Wang, L., Essene, E. and Zhang, Y. (1999) Mineral inclusions in pyrope crystals from garnet ridge, Arizona, USA: Implications for processes in the upper mantle. *Contributions to Mineralogy and Petrology*, **135**, 164–178.

Wang, L., Rouse, R., Essene, E., Peacor, D. and Zhang, Y. (2000) Carmichaelite, a new hydroxyl-bearing titanite from garnet ridge, Arizona. *American Mineralogist*, **85**, 792–800.

[*Manuscript received 27 July 2004: revised 22 April 2005*]